

# Estimation of fire-induced CO plume age from NAST-I during the FIREX-AQ field campaign

Daniel K. Zhou<sup>1</sup>,\* Allen M. Larar, Xu Liu, and Xiaozhen Xiong

NASA Langley Research Center, Hampton, Virginia, United States

**Abstract.** Ultra-spectrally resolved infrared measurements from aircraft and space-based observations contain information about tropospheric carbon monoxide (CO) and ozone (O<sub>3</sub>), as well as other trace species. A methodology for retrieving these tropospheric trace species from such remotely sensed spectral data has been developed and validated for the National Airborne Sounder Testbed-Interferometer (NAST-I). The Fire Influence on Regional to Global Environments and Air Quality (FIREX-AQ) field campaign was conducted during August 2019 to investigate the impact of wildfire and biomass smoke on air quality and weather in the continental United States. NAST-I CO and O<sub>3</sub> measurements from the recent FIREX-AQ field campaign are presented and used to estimate wildfire plume age. Results show enhanced levels of CO in the evolving plume as it is transported away from the fire ground site, and its plume age is associated with the plume distance in both the vertical and horizontal directions from the wildfire location. These results are enabled by the moderate-vertical and high-horizontal resolution obtained from the NAST-I IR spectrometer onboard the NASA ER-2 aircraft. This study advances our knowledge of fire-induced plumes with their evolution and age characterized in three-dimensional space using information from NAST-I retrieved CO and O<sub>3</sub> and relative changes in their concentrations. © The Authors. Published by SPIE under a Creative Commons Attribution 4.0 International License. Distribution or reproduction of this work in whole or in part requires full attribution of the original publication, including its DOI. [DOI: [10.1117/1.JRS.16.034522](https://doi.org/10.1117/1.JRS.16.034522)]

**Keywords:** plume age; ozone; carbon monoxide; wildfires; infrared measurements; remote sensing.

Paper 220099L received Feb. 18, 2022; accepted for publication Aug. 3, 2022; published online Aug. 22, 2022.

## 1 Introduction

In recent decades, wildfires have gained more of our attention as their number of occurrences, sizes, and intensities have significantly increased, likely due to dryer and hotter conditions from climate change. Wildfire-induced pollutants and smoke (i.e., poor air quality) pose great risks to human health, although wildfires can be an important natural event in many ecosystems. The chemistry and composition of smoke from wildfires are being studied to improve our understanding of the relationship between combustion and air quality, weather, and climate and the ability to forecast.<sup>1</sup>

Carbon monoxide (CO) is one of the major pollutants due to combustion.<sup>2</sup> The significance of CO in atmospheric chemistry was recognized long ago when a photo-chemically driven chain reaction was recognized linking the tropospheric cycles of CO, methane (CH<sub>4</sub>), and ozone (O<sub>3</sub>) with those of the hydroxyl radical (OH) and hydroperoxyl radical (HO<sub>2</sub>).<sup>3</sup> O<sub>3</sub> is another major pollutant that can also cause several health problems to human beings.<sup>4</sup> O<sub>3</sub> plays a significant role in tropospheric chemistry; details on ozone production from wildfires can be found in other studies.<sup>5,6</sup> Previous studies and observations have suggested some degree of O<sub>3</sub> production as wildfires generate emissions of O<sub>3</sub> precursors, such as NO<sub>x</sub> (NO + NO<sub>2</sub>) emitted from wildfires and thus increasing peroxyacetyl nitrate (PAN) as well.<sup>6</sup> O<sub>3</sub> production decreases quickly downwind of combustion.<sup>7</sup> However, O<sub>3</sub> production can be complicated and depends upon many factors, e.g., aerosols in a biomass plume from a wildfire reduce the photolysis rates of NO<sub>2</sub> and O<sub>3</sub>. The impact of lower photolysis rates on O<sub>3</sub> production is not clear. Reducing the photolysis rates can either increase or decrease the net O<sub>3</sub> production by changing both the O<sub>3</sub>

\*Address all correspondence to Daniel K. Zhou, [daniel.k.zhou@nasa.gov](mailto:daniel.k.zhou@nasa.gov)

production and loss rates.<sup>6</sup> O<sub>3</sub> plume characteristics from wildfires are not as obvious as that for CO plumes because O<sub>3</sub> is not directly produced by wildfires, and it has a short lifetime in comparison with that of CO. However, both CO and O<sub>3</sub> within wildfire plumes are particularly interesting as they are related to the plume age and associated plume evolution and transport. Observations were made of  $\Delta\text{O}_3/\Delta\text{CO}$  due to wildfires for biome and plume age,<sup>6</sup> indicating a positive relationship between  $\Delta\text{O}_3/\Delta\text{CO}$  and plume age. Tropospheric chemical reactions involving CO extend their influence on air quality and global climate through accumulation of greenhouse gases. CO can be transported a great distance from its original source due to its relatively long lifetime (averaging about 2 months) in the troposphere.

The Fire Influence on Regional to Global Environments and Air Quality (FIREX–AQ) experiment in August 2019 is the first joint field campaign conducted by NOAA and NASA addressing wildfire emissions and their impact on air quality and climate. It was dedicated to the sampling and characterization of fires and their impact on air quality and weather from the point of trace species emissions.<sup>8,9</sup> Ground, airborne, and satellite measurements were made during the FIREX–AQ field phase. The National Airborne Sounder Testbed-Interferometer (NAST–I) is an airborne interferometer sounding system. It provides a highly spatial linear resolution that is equal to 13% of the aircraft altitude at nadir and 13 instrument instantaneous fields-of-view (IFOVs) across the aircraft track from 13 scan angles (i.e., 2.6-km IFOV,  $\sim 3.4$  km apart on the ground from an ER-2 altitude of 20 km). NAST–I spatially scans and provides high-spectral resolution ( $0.25\text{ cm}^{-1}$ ) measurements within the spectral region of 645 to  $2700\text{ cm}^{-1}$ .<sup>10–15</sup> Here, we use measurements from NAST–I on board the NASA ER–2 aircraft to study fire-induced CO plumes. NAST–I continuously covers a space large enough to monitor the wildfire plume from its origination, evolution and transport, providing three-dimensional (3D) distributions of geophysical parameters including O<sub>3</sub> and CO with a higher spatial resolution compared with satellite IR-ultraspectral sensors, and thus, it benefits our study of wildfire plumes.<sup>16</sup> NAST–I data used in this study were collected under clear-sky conditions. Geophysical parameters cannot be retrieved with NAST–I under opaque clouds as infrared measurements are not able to penetrate opaque clouds.<sup>14</sup> Materials presented in this study are a follow-up to the work of Zhou et al.<sup>16</sup> A brief description of the FIREX–AQ experiment, observations, and wildfire plume age estimation methodology is given in Sec. 2. Results and discussion are presented in Sec. 3. Summary and concluding remarks follow in Sec. 4.

## 2 Experiment, Observation, and Plume Age Estimation Methodology

FIREX–AQ is a multi-disciplinary effort campaign with multi-agency collaborations to study complex fire systems. Research platforms were heavily instrumented with *in-situ* and remote-sensing devices to allow for exhaustive characterization of gases and aerosols, optical properties, wind fields, fire radiative power, and more. Ground-based examinations of fuels and burned areas permitted clearer connections between atmospheric pollutants and their sources. Modeling efforts were used during the campaign to predict transport and study emissions and downwind plume transformations.

The results presented here are based upon CO and O<sub>3</sub> retrievals from NAST–I measurements. The NAST–I instrument and its retrieval algorithms are described elsewhere.<sup>10–19</sup> The western portion of the FIREX–AQ campaign domain (August 5, 2019, to August 21, 2019) covers 14 large wildfires fueled by grass, woodland, and scrub.<sup>20</sup> Fire-induced CO plumes observed by NAST–I during the FIREX–AQ have been analyzed and reported.<sup>16</sup> For this study of wildfire plume age, we chose the ER–2 sorties over the William Flats fire and the extended downwind area from August 7, 2019, as the ER-2 sorties have  $\sim 450$ -km downwind flight leg segments. The William Flats fire was caused by lightning on August 2, 2019. It covered  $\sim 100\text{ km}^2$  and was located about 11-km southeast of Keller, Washington. The ER–2 flew from west ( $-120^\circ$  longitude) to east ( $-113^\circ$  longitude) and then back west at a near-constant latitude, passing over the fire location ( $48.0^\circ$  latitude,  $-118.5^\circ$  longitude) and the extended downwind area to detect fire-induced gas emissions and characterize their subsequent evolution. A large downwind area covered by the ER–2 flight makes an excellent naturally occurring experiment to study fresh and aged plumes.

Geophysical parameters such as temperature, moisture, and CO and O<sub>3</sub> profiles are retrieved from NAST-I measured spectral radiances. The NAST-I retrieval algorithm was developed, tested, improved, and validated.<sup>13,14,17</sup> The NAST-I trace gas (CO and O<sub>3</sub>) retrieval algorithm was also developed<sup>18</sup> and later improved by implementation of a surface emissivity retrieval.<sup>19</sup> During the FIREX-AQ field campaign, CO retrievals are validated using *in-situ* measurements from the NASA DC-8 aircraft.<sup>16</sup> There are two O<sub>3</sub> *in-situ* sensors flying on the DC-8 aircraft: one is the NOAA nitrogen oxides and ozone (NO<sub>y</sub>O<sub>3</sub>) 4-channel chemiluminescence instrument<sup>21</sup> and the other is the rapid ozone experiment (ROZE).<sup>22</sup> The nature of O<sub>3</sub> (e.g., its lifetime and photochemical reactions) and its impact on the atmosphere from wildfires is not as obvious as that of CO. O<sub>3</sub> is relatively stable in comparison with fire-induced CO, which makes it a bit easier for inter-comparison between NAST-I remotely sensed and *in-situ* measured ozone. A few DC-8 sorties were spatially coincident with the ER-2 sorties at the same fire locations, but, in general, they had lag times of a few hours. There was one exception wherein both spatial and temporal coincidence was achieved between the two aircraft, specifically, on August 6, 2019.<sup>16</sup> Here, we use the 60-s merged data from DC-8 measurements available from the FIREX-AQ database<sup>23</sup> to compare with NAST-I O<sub>3</sub> retrievals. An inter-comparison between ER-2 NAST-I O<sub>3</sub> and DC-8 *in-situ* O<sub>3</sub> is made in the vicinity of the William Flats fire location from data collected on August 6, 2018, to August 8, 2019. Figure 1(a) plots the NAST-I O<sub>3</sub> (in black open circles) and *in-situ* O<sub>3</sub> data (the mean of ROZE and NO<sub>y</sub>O<sub>3</sub> measurements, in black asterisks) with a coincidence spatial-criteria of  $|\Delta(\text{latitude})| < 0.05^\circ$  and  $|\Delta(\text{longitude})| < 0.05^\circ$  and temporal-criteria of  $|\Delta(\text{UTC})| < 1$  h for August 6, 2019. The NAST-I O<sub>3</sub> profile is interpolated to DC-8 *in-situ* altitude. Figure 1(b) shows the difference between NAST-I and *in-situ* O<sub>3</sub> plotted in Fig. 1(a). Similar data from August 7 and August 8, 2019, are also plotted (in red and blue symbols, respectively) with a relatively larger temporal-criteria of  $|\Delta\text{UTC}|$  as shown in Fig. 1(c). Overall, from the data shown in Fig. 1, the mean error (bias) and standard deviation error (STDE) between NAST-I retrievals and *in-situ* measurements are 7.55 (ppbv) and 10.85 (ppbv), respectively. Reasonable agreement between the ER-2 NAST-I and DC-8 *in-situ* O<sub>3</sub> measurements is achieved with some differences due to their spatial and temporal mismatches. However, it is noticed that NAST-I O<sub>3</sub> starts to deviate from *in-situ* measurements at an altitude of  $\leq 3$  km. This is believed to be a consequence of the expected lower ozone retrieval sensitivity in the NAST-I passive infrared measurements at an altitude region below 3 km. However, the uncertainty of  $\Delta\text{O}_3$  is relatively small compared with that of O<sub>3</sub> itself as the retrieval uncertainties of the polluted and clean background O<sub>3</sub> regions are similar. From this

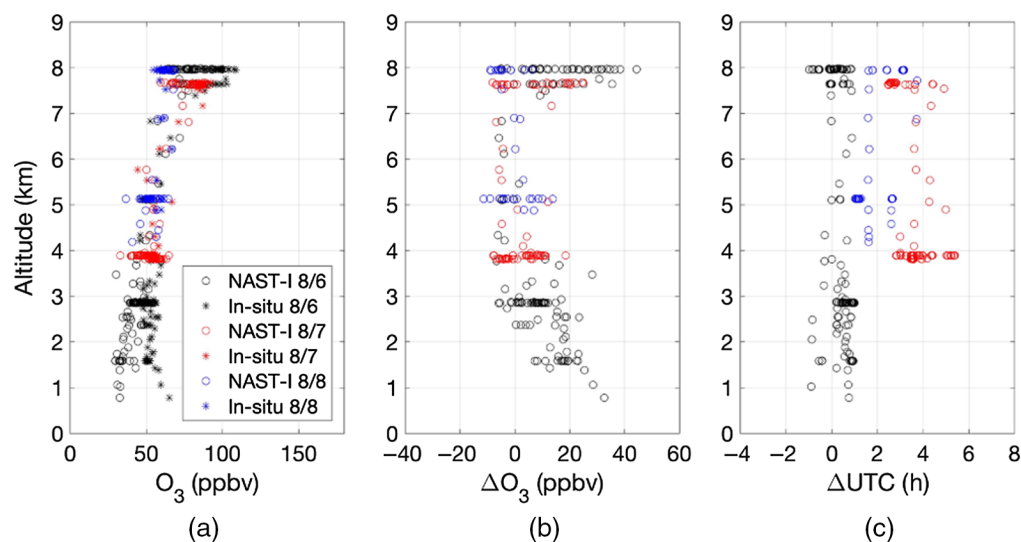


**Fig. 1** NAST-I O<sub>3</sub> retrieval evaluation with *in-situ* measurements near the William Flats fire location from August 6, 2019, to August 8, 2019, in black, red, and blue, respectively (see text). (a) NAST-I retrieved and *in-situ* measured O<sub>3</sub>; (b) the difference between NAST-I and *in-situ* O<sub>3</sub>; and (c) the UTC difference between NAST-I and *in-situ* O<sub>3</sub> measurements.

evaluation, we believe that NAST-I  $O_3$  retrievals are reasonably good at the altitude of 3 km and above and can be used together with CO retrievals to estimate the age of wildfire-induced plumes as presented in the following section.

The William Flats fire progression and CO plume evolution during August 6, 2019, to August 8, 2019, were observed by multiple airborne sensors including NAST-I.<sup>16</sup> NAST-I CO retrieval uncertainty has been evaluated with the co-incident *in-situ* measurements and found to have a bias of  $\sim 8$  ppbv and STDE of  $\sim 28$  ppbv.<sup>16</sup> The NAST-I measurements provide 3D distribution of temperature, water vapor, CO, and  $O_3$ . For the case study here, the ER-2 sorties went over the William Flats fire and the extended downwind area twice. NAST-I retrieved cross sections in nadir view are plotted in Fig. 2 for one sortie (from west to east); the retrievals from the return sortie are almost identical. Moisture layers are shown in relative humidity (RH) with less saturation ( $< 100\%$ ), indicating clear-sky conditions in the observations. CO plumes in the downwind area are evidently clear. The  $O_3$ , plotted in a logarithmic scale, illustrates its small variation in free troposphere from the ground level up and its enhancement over the fire location ( $-118.5^\circ$  longitude).

Fire-induced plumes contain information on chemical gaseous photochemical reaction and production; it is essential to know the plume's evolution and age to better understand impacts to air quality, weather, and climate. Fire plume age has been widely measured and studied by numerous researchers. Observations of  $\Delta O_3/\Delta CO$  due to wildfires by biome and plume age were summarized by Jaffe and Wigder.<sup>6</sup> Many factors contribute to  $O_3$  production within wildfire plumes. In general, Jaffe and Wigder found a positive relationship between the  $\Delta O_3/\Delta CO$  ratio and plume age. Here, we assume this relationship is a linear  $T = \alpha R + \beta$ , where  $T$  is plume age in hours and  $R$  is  $\Delta O_3/\Delta CO$  ratio.  $\alpha$  and  $\beta$  are the slope and intercept, respectively. A fitting relationship is obtained from Table 1 of Jaffe and Wigder.<sup>6</sup> For boreal and temperate regions (BTR),  $\alpha = 327.2$  and  $\beta = 89.4$ , whereas for the tropical and subtropical regions (TSR),  $\alpha = 215.8$  and  $\beta = 3.1$ . The  $\Delta O_3/\Delta CO$  ratio increases as the plume ages, and it ages relatively

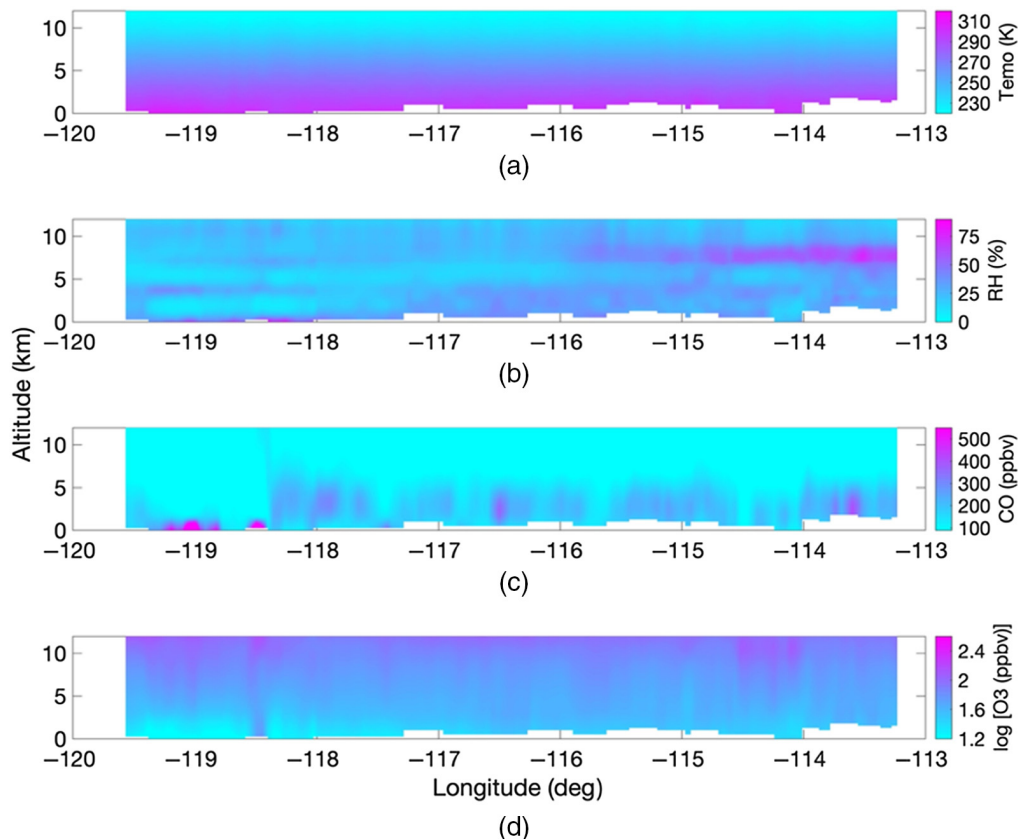


**Fig. 2** NAST-I retrieval cross sections in nadir view for (a) temperature (K); (b) RH (%); (c) CO (ppbv); and (d)  $O_3$  (ppbv) in logarithmic scale.

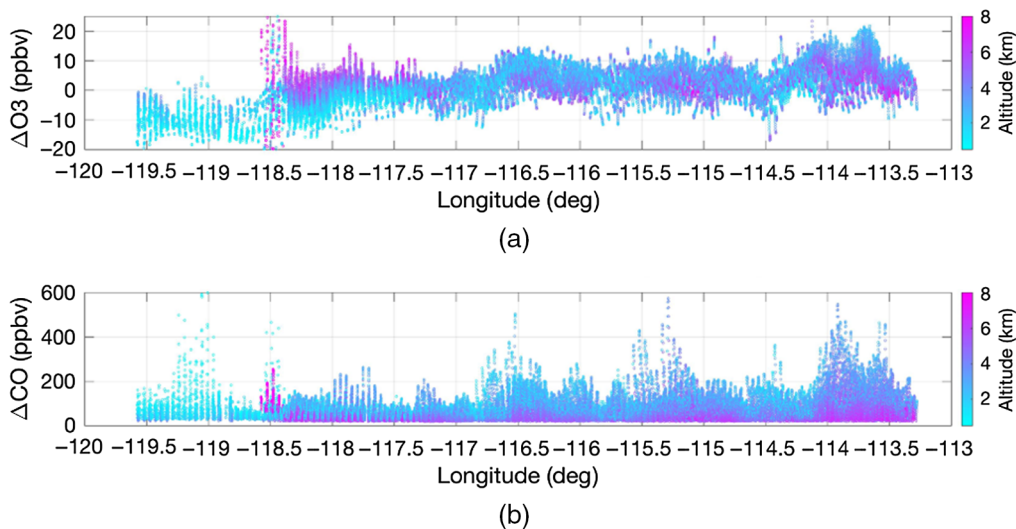


**Fig. 3** (a)  $\Delta O_3$  and (b)  $\Delta CO$  distribution within the fire-induced plumes.

slower in tropical and equatorial regions as more  $O_3$  production is expected from more  $NO_x$  emissions per unit of fuel consumed.<sup>6</sup> Based upon this assessment, our plume age estimation methodology relies on  $\Delta O_3/\Delta CO$  ratios within the plumes.

Within fire-induced CO plumes, we assume that CO concentrations are greater than 135 ppbv. Subtracting the background estimates,  $\Delta O_3$  and  $\Delta CO$  are calculated using NAST-I retrieved  $O_3$  and CO.  $O_3$  background is assumed to be the average of its regional climatology, which is from a global climatology database that consists of 15,150 profiles obtained from the extended SeeBor database of the University of Wisconsin–Madison<sup>23,24</sup> and NAST-I retrieval mean, whereas CO background is assumed to be its regional climatology. 3D distributions of  $\Delta O_3$  and  $\Delta CO$  within the plumes (where  $CO > 135$  ppbv) are plotted in Figs. 3(a) and 3(b), respectively, along the longitude with a color distribution in altitude. It is noted that elevated  $O_3$  spans at least 26 km near the fire location ( $-118.5^\circ$  longitude) and covers an area of 531 km<sup>2</sup>. It is worth mentioning that  $\Delta O_3$  and  $\Delta CO$  plotted in Fig. 3 are estimations as the  $O_3$  and CO background within the plumes is not precisely known but is estimated to the best of our knowledge and assumed to be the same throughout the local region.

### 3 Results and Discussion

The  $\Delta O_3/\Delta CO$  ratio is estimated from retrievals using NAST-I flight observations and is plotted in Fig. 4(a). CO plume age can be simply projected from wildfire  $\Delta O_3/\Delta CO$ . For the William Flats fire location ( $48^\circ$  latitude), a linear combination of 55% BTR and 45% TSR coefficients are used to calculate the plume age that would reflect a near fresh plume at the fire location. Estimated plume age is plotted in Fig. 4(b). For plumes at a lower altitude (i.e., 4 km and below), their ages increased as the plumes moved away from the fire location downwind and merged with aged plumes ( $\sim 60$  to 100 h), whereas other aged plumes were sitting at a higher altitude (4 km and above).

Figure 5(a) plots the plume age along the longitude with error bars indicating its variation over altitude and longitude. Fresh plumes were observed to be closer to the fire location, whereas aged plumes were in the downwind regions as expected. Figures 5(b)–5(c) plots the mean plume age against the altitude with an error bar indicating its variation over longitude and latitude. The ages depend on the distance (e.g., longitude) from the fire location. Figure 5(b) covers all data shown in Fig. 5(a); Figs. 5(c) and 5(d) have data plotted with longitude that is  $< -117^\circ$  and  $> -117^\circ$ , respectively. Near the fire location, shown in Fig. 5(c), fresh plumes are at a lower altitude, and plume ages increase as altitude increases. As the plumes move further downwind, as shown in Fig. 5(d), fresh and aged plumes were mixed along the altitudes with a near constant mean plume age of  $\sim 50$  h, but with a large variation (i.e., a large standard deviation) indicated

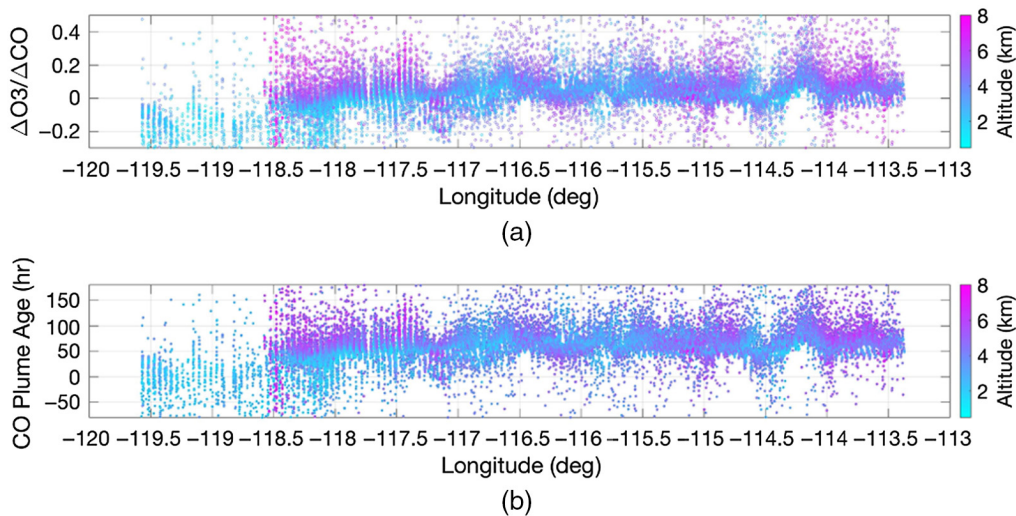


**Fig. 4** (a)  $\Delta O_3/\Delta CO$  distribution along the longitude within the fire-induced plumes and (b) estimated plume age distribution.

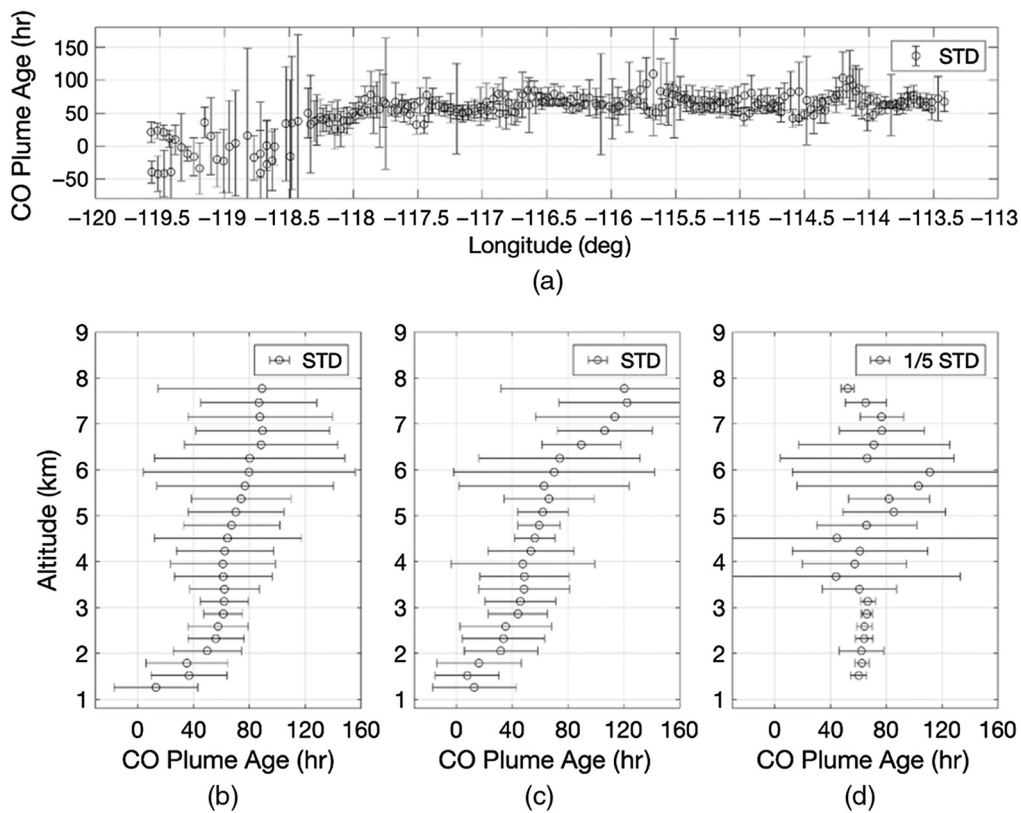


**Fig. 5** (a) Plume age distribution along the longitude. Plume age distribution along the altitude: (b) all data shown from (a); (c) data from longitude <  $-117^\circ$  (near the fire location); and (d) data from longitude >  $-117^\circ$  (farther away from the fire location).

by the error bars (reduced by a factor of 5 for clarity) in the altitude region of  $\sim 3.5$  to 7 km, where a greater mixture of fresh and aged plumes co-exists. In general, as shown in Fig. 4(b), fresh plumes were at a lower altitude, whereas aged plumes were found in the upper regions. Finally, the distributions of enhanced CO column density from the fire plume and the vertical mean CO plume age (VMCOPA) are plotted in Figs. 6(a) and 6(b), respectively. It is worth noting that there are two flight tracks (two legs) back and forth with time evolution on top of each other; only

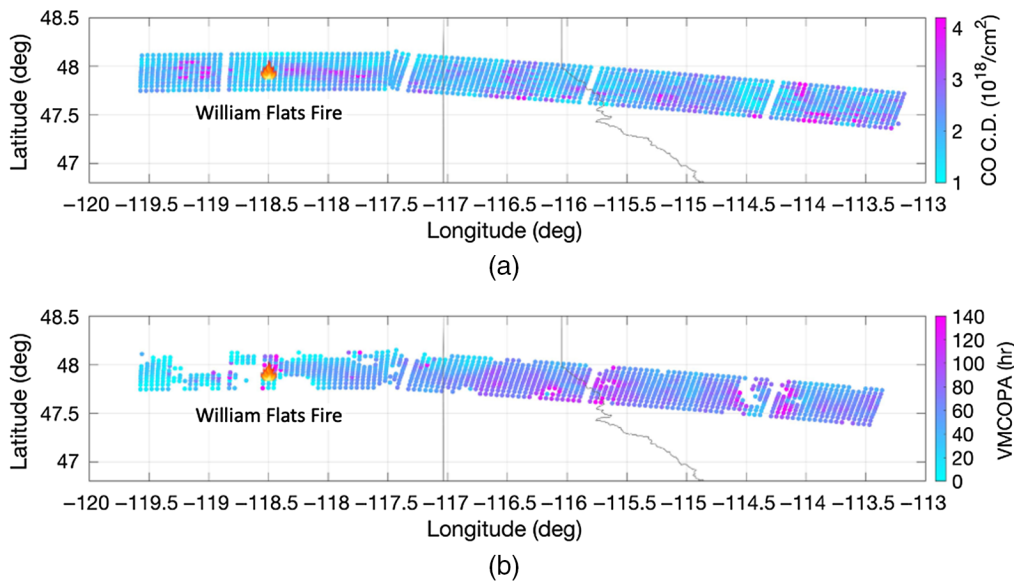


**Fig. 6** Distribution of (a) CO column density and (b) VMCOPA.

the first leg is plotted in Fig. 6 for clarity. Comparing CO column density and its vertical mean CO plume age, a large amount of relatively fresh CO plumes was near the fire location and aged CO plumes was transported further downwind and/or to the upper regions.

The William Flats fire started on August 2, 2019, and the oldest plumes could be 4 to 5 days old. The plume ages could be from mixed plumes (or effective plumes) as indicated in Figs 4-6; therefore, in the area farthest away from the fire location, they could be somewhat <5 days old in our estimations. Nevertheless, the plume age distributions, both horizontally and vertically (shown in Figs. 5-6), make sense for the way plumes are transported and aged. The error or uncertainty of plume age derived here is largely due to (1)  $\text{O}_3$  and CO retrieval error, especially at lower altitudes (3 km and below) as retrieval sensitivity decreased; (2) the uncertainty from estimated CO and  $\text{O}_3$  background within the plume; (3) the limited data available for deriving the relationship between the plume age and  $\Delta\text{O}_3/\Delta\text{CO}$  ratio and a large data scattering and uncertainty in the dataset;<sup>6</sup> (4) a linear fitting relationship between the plume age and  $\Delta\text{O}_3/\Delta\text{CO}$  ratio may not be the best representation; and (5) mixed (or effective) plumes being assessed possibly contain contributions from multiple fire sources, especially in locations further away from the primary fire location.

Currently these error sources are not completely quantified; therefore, the plume age presented in this letter study is only an estimation. Regardless, it is critically important even though it may lack some quantitative accuracy because it nicely demonstrates the ability to characterize wildfire plumes and estimate their age from the perspective of an advanced ultraspectral infrared remote sounder. CO and  $\text{O}_3$  retrievals are the mean over the IFOV with a vertical column resolution. The plume that we dealt with is an effective plume or a volume mean of mixed plumes. The plume age presented herein is also an effective mean plume age in the NAST-I sensor IFOV, which can be different from *in-situ* measurements.

It is worth mentioning that the North Hills fire, started on July 26, 2019, was located at about 5 km northwest of Lake Helena, Montana (46.8° latitude, -112° longitude). It covered  $\sim 20 \text{ km}^2$ . CO plumes from the North Hills fire are unlikely but could contribute to the data presented here at the locations near the western (possibly upwind) areas of the North Hills fire location.

#### 4 Summary and Concluding Remarks

The FIREX-AQ field campaign with multiple aircraft *in-situ* and remotely sensed observations provides characterization of distributions of chemical species induced by wildfire emissions and subsequent evolution. This unique dataset is very much desirable in validating NAST-I  $\text{O}_3$  and CO retrievals and illustrating the benefits of such data for wildfire characterization. The wildfire

case of Williams Flats from the FIREX–AQ experiment reported herein is used to demonstrate a fire-induced plume age estimation approach. Several major summary items and conclusions can be obtained from this work. (1) NAST–I remotely sensed  $O_3$  is evaluated by favorable inter-comparisons with the *in-situ*  $O_3$  measurements, which show a positive agreement (shown in Fig. 1). (2) Small but significant enhanced  $O_3$  production near the William Flats wildfire location is observed by NAST–I. (3)  $O_3$  and CO productions impacted by the wildfire are estimated within the fire-induced plume. (4) Plume age is estimated using NAST–I observed  $\Delta O_3/\Delta CO$  ratios and a linear fitting relationship from previous observations of wildfire  $\Delta O_3/\Delta CO$  ratios by biome and plume age.<sup>6</sup> (5) Plume age distribution both horizontally and vertically indicates the plume ages as it moves away from the fire location (for William Flats Fire case).

It was reported earlier that first-of-a-kind wildfire-induced plume measurements were obtained by the NAST–I ultraspectral remote sensor on board the ER–2 suborbital aircraft, which shows the intensity and size of wildfire plumes in a high-spatial-resolution of 2.6 km. Now, in the present study, the plume age estimation in a 3D high-spatial-resolution adds critical temporal information of the fire-induced plume, demonstrating the capability of an ultraspectral remote sensor such as NAST–I with a higher spectral and spatial resolution to monitor CO and  $O_3$  and its advantage of giving broader spatial and temporal assessment by rapidly covering a large field of observation. This work demonstrates 3D plume age estimation and advances our measurement ability to observe fire-induced plumes and characterize their evolution and age.

NAST–I was successfully operated during all ER–2 flights of the FIREX–AQ experiment (a total of 11 flights and 50+ h of science data collected). NAST–I retrievals (e.g., atmospheric temperature, relative humidity, CO, and  $O_3$  profiles, also surface skin temperature), together with experiment data from other satellite/aircraft/ground measurements and analysis from the FIREX–AQ campaign, are available<sup>25</sup> for the science community to study wildfire-related topics as described by the overarching objective of the FIREX–AQ experiment<sup>8</sup> and beyond.

## Acknowledgments

The authors greatly appreciate the FIREX–AQ management team and the aircraft pilots and crew of NASA ER–2 and DC–8.  $O_3$  *in-situ* data were provided by the ROZE team (Principal Investigators Drs. R. A. Hannun and T. F. Hanisco) and the NOAA  $NO_yO_3$  team (Principal Investigator Dr. T. B. Ryerson). The authors wish to thank A. M. Noe of NASA Langley Research Center and L. Rochette of LR Tech, Inc. for their dedicated support of the NAST–I instrument upgrade, maintenance, and field mission. The authors wish to thank Dr. J. A. Kaye of the NASA Science Mission Directorate and Dr. M. D. Goldberg of NOAA NESDIS for their continued support of the NAST–I program. The authors wish to thank one anonymous referee for his/her useful comments and suggestions. The NAST–I is part of the Airborne Science Program within the NASA Earth Science Division.

## References

1. P. J. Crutzen et al., “Biomass burning as a source of atmospheric gases CO,  $H_2$ ,  $N_2O$ , NO,  $CH_3Cl$ , and COS,” *Nature* **282**, 253–256 (1979).
2. J. Fishman et al., “Identification of widespread pollution in the Southern Hemisphere deduced from satellite analyses,” *Science* **252**, 1693–1696 (1991).
3. H. Levy, II, “Natural atmosphere: large radical and formaldehyde concentrations predicted,” *Science* **173**, 141–143 (1971).
4. J. J. Zhang, Y. Wei, and Z. Fang, “Ozone pollution: a major health hazard worldwide,” *Front. Immunol.* **10**, 2518 (2019).
5. H. B. Singh et al., “Pollution influences on atmospheric composition and chemistry at high northern latitudes: boreal and California forest fire emissions,” *Atmos. Environ.* **44**, 4553–4564 (2010).
6. D. A. Jaffe and N. L. Wigder, “Ozone production from wildfires: a critical review,” *Atmos. Environ.* **51**, 1–10 (2012).



7. E. V. Fischer et al., “Meteorological controls on observed peroxyacetyl nitrate at Mount Bachelor during the spring of 2008,” *J. Geophys. Res.* **115**, D03302 (2010).
8. “FIREX–AQ: investigating smoke from wildfire and biomass burning,” <https://www.esrl.noaa.gov/csl/projects/firex-aq/> (accessed 5 Nov 2021).
9. D. A. Jaffe et al., “Wildfire and prescribed burning impacts on air quality in the United States,” *J. Air Waste Manage. Assoc.* **70**, 583–615 (2020).
10. “The National Airborne Sounder Testbed-Interferometer (NAST-I),” <https://airbornescience.nasa.gov/instrument/NAST-I> (accessed 5 Nov. 2021).
11. D. Cousins and W. L. Smith, “National Polar-Orbiting Operational Environmental Satellite System (NPOESS) Airborne Sounder Testbed-Interferometer (NAST-I),” *Proc. SPIE* **3127**, 323–331 (1997).
12. W. L. Smith et al., “NAST-I: results from revolutionary aircraft sounding spectrometer,” *Proc. SPIE* **3756**, 2–8 (1999).
13. D. K. Zhou, W. L. Smith, and A. M. Larar, “Tropospheric ozone near-nadir-viewing IR spectral sensitivity and ozone measurements from NAST-I,” *Proc. SPIE* **4151**, 277–284 (2001).
14. D. K. Zhou et al., “Thermodynamic product retrieval methodology for NAST-I and validation,” *Appl. Opt.* **41**, 6957–6967 (2002).
15. A. M. Larar et al., “IASI spectral radiance validation inter-comparisons: case study assessment from the JAIVEx field campaign,” *Atmos. Chem. Phys.* **10**, 411–430 (2010).
16. D. K. Zhou et al., “Wildfire-induced CO plume observations from NAST-I during the FIREX–AQ field campaign,” *IEEE J. Sel. Top. Appl. Earth Observ. Remote Sens.* **14**, 2901–2910 (2021).
17. D. K. Zhou et al., “Physically retrieving cloud and thermodynamic parameters from ultra-spectral IR measurements,” *J. Atmos. Sci.* **64**, 969–982 (2007).
18. D. K. Zhou et al., “Tropospheric CO observed with the NAST-I: retrieval methodology, analyses, and first results,” *Appl. Opt.* **44**, 3032–3044 (2005).
19. D. K. Zhou et al., “Global land surface emissivity retrieved from satellite ultraspectral IR measurements,” *IEEE Trans. Geosci. Remote Sens.* **49**, 1277–1290 (2011).
20. J. Schwarz and the FIREX-AQ Science Team, “The FIREX-AQ 2019 dataset is public,” in *EGU General Assembly 2020, 4–8 May 2020, EGU2020-20755* (2020).
21. “NOAA Nitrogen Oxides and Ozone (NO<sub>y</sub>O<sub>3</sub>) instrument,” <https://airbornescience.nasa.gov/instrument/NOyO3> (accessed 5 Nov. 2021).
22. “NASA Rapid OZone Experiment (ROZE),” <https://airbornescience.nasa.gov/instrument/ROZE> (accessed 5 Nov. 2021).
23. E. E. Borbas et al., “Global profile training database for satellite regression retrievals with estimates of skin temperature and emissivity,” in *Proc. Int. ATOVS Study Conf. XIV, Beijing, China, CIMSS, University of Wisconsin–Madison*, pp. 763–770 (2005).
24. S. W. Seemann et al., “Development of a global infrared land surface emissivity database for application to clear-sky sounding retrievals from multi-spectral satellite radiance measurements,” *J. Appl. Meteorol. Clim.* **47**, 108–123 (2008).
25. “NOAA/NASA FIREX–AQ campaign data archive,” <https://asdc.larc.nasa.gov/project/FIREX-AQ> (accessed 5 Nov. 2021).

**Daniel K. Zhou** received his PhD in physics from Utah State University, Logan, in 1992. Currently, he is the principal investigator for the NAST-I airborne instrument and a physical scientist within the science directorate of NASA Langley Research Center. He has more than 30 years of research experience with hyperspectral interferometer remote sensors, measurements, retrieval algorithms, data processing, and applications. He was the recipient of the NASA Exceptional Achievement Medal and Exceptional Service Medal.

**Allen M. Larar** received his PhD in atmospheric and space sciences from the University of Michigan, Ann Arbor, in 1993. Currently, he is an associate director for Research and Mission Science within the Science Directorate at NASA Langley Research Center. He has more than 30 years of experience in advancing passive remote sensing measurement capabilities focusing on characterizing atmospheric thermodynamic state and trace species composition. He was the recipient of the NASA Exceptional Service Medal.

**Xu Liu** received his PhD in physical chemistry from the University of Denver, Denver, Colorado, in 1989. Currently, he is a senior research scientist at Science Directorate, NASA Langley Research Center. His research interests include fast radiative transfer model and retrieval algorithm development for both passive and active remote sensing instruments ranging from microwave to visible spectral range. He was the recipient of the NASA Exceptional Achievement Medal and Exceptional Scientific Achievement Medal.

**Xiaozhen Xiong** received his PhD in atmospheric sciences from the University of Alaska, Fairbanks, in 2000. Currently, he is a research scientist at Science Directorate of NASA Langley Research Center. Prior to joining NASA in 2020, he was a scientist supporting NOAA/NESDIS/STAR activities. He has comprehensive experiences from the IR and UV sensor calibration, fast radiative transfer modeling, and retrieval algorithm development, as well as the remote sensing of polar cloud and surface properties.